Chinese Chemical Letters 36 (2025) 110497

Contents lists available at ScienceDirect

Chinese Chemical Letters

journal homepage: www.elsevier.com/locate/cclet

High quantum yield yellow emission carbon dots for the construction of blue light blocking films

Liwen Wang[a], Boyang Wang[b], Siyu Lu[b,*], Shubo Lv[a,*], Xiaoli Qu[c,*]

[a] Neonatal Disease Screening Unit, The Third Affiliated Hospital of Zhengzhou University, Zhengzhou 450001, China
[b] College of Chemistry, Pingyuan Laboratory, Zhengzhou University, Zhengzhou 450001, China
[c] Erythrocyte Biology Laboratory, School of Life Sciences, Zhengzhou University, Zhengzhou 450001, China

ARTICLE INFO

Article history:
Received 5 August 2024
Revised 18 September 2024
Accepted 23 September 2024
Available online 24 September 2024

Keywords:
Carbon dots
High quantum yield
Controllable preparation
Blue light blocking
Composite film

ABSTRACT

White light illumination is essential in daily life, however, the substantial amount of blue light it contains can damage human eyes. Therefore, it is important to block this high-energy blue light to protect visual health. In this study, yellow-emitting carbon dots (CDs) with a quantum yield exceeding 94% were synthesized using citric acid and urea. These CDs effectively absorb blue light. By incorporating them into polystyrene, multiple films termed CDs-based blue light blocking films (CBFs) were developed, each offering different levels of blue light absorption. These CBFs exhibited excellent transparency and efficient blue light filtering capabilities. This study highlights the potential of high quantum yield CDs, which specifically absorb blue light, as foundational materials for developing light-blocking solutions against high-energy short-wavelength light.

In contemporary society, electronic devices such as computers and smartphones are essential, influencing every aspect of daily life from work to leisure. These devices predominantly utilize white light-emitting diodes (WLEDs) for screens and lighting due to their efficiency, energy-saving benefits, and durability. However, a key drawback of WLEDs is their emission of cool white light, which contains high levels of blue light intensity. Several studies have indicated that extended exposure to blue light can negatively impact human health, causing issues such as eye strain, retinal damage, photodynamic damage to aging lenses, and potential macular degeneration. These concerns are increased in the digital era, where frequent use of electronic devices has become widespread, contributing to a rise in eye problems linked to blue light exposure [1-3].

Various strategies have been investigated to reduce the detrimental effects of blue light [4], such as the use of blue and UV cutoff filters, antioxidants, blue-light-reducing intraocular lenses, and blue-light-blocking films [5]. However, these solutions are still constrained by factors such as dependency on the angle of light incidence, inadequate blocking efficiency, poor transparency, and long-term instability [6]. Therefore, there is an urgent need for more effective, reliable, and versatile blue light protection technologies. Photoluminescent materials are being considered as potential options due to their capability to absorb high-energy blue light and convert it into less harmful wavelengths. Rare earth elements, semiconductor quantum dots, and carbon dots (CDs) are the primary focus of research in this field [7-10]. However, the high cost and limited renewability of rare earth elements, as well as the toxicity associated with cadmium-containing quantum dots, present substantial challenges. In contrast, CDs offer numerous advantages, such as easy synthesis, tunable optical properties, diverse sources, non-toxicity, and renewability. These attributes make CDs particularly attractive for applications in blue light protection [11-13].

Blue light-blocking CDs must absorb light in the blue region, which requires them to emit yellow light [14-16]. For instance, Zhao *et al.* produced concentration-dependent CDs derived from biomass. These CDs were then combined with polyvinyl alcohol (PVA) to form optical blocking films capable of effectively blocking short-wavelength light [17]. Developing CDs with high quantum yields is advantageous for blue light-blocking materials as it enhances their ability to absorb incident light. Han *et al.* synthesized biomass-derived CDs with a quantum yield of 10%, which, when combined with PVA, effectively absorbed short-wavelength light [18]. Furthermore, Guo *et al.* developed yellow-light-emitting CDs with a high quantum yield of 71% using ethylenediamine and 1-amino-2-naphthol-4-sulfonic acid as precursors [19]. When integrated into PVA, these CDs were used to prepare flexible films that

* Corresponding authors.
E-mail addresses: sylu2013@zzu.edu.cn (S. Lu), 13939017963@163.com (S. Lv), qv1110xiaoli@126.com (X. Qu).

https://doi.org/10.1016/j.cclet.2024.110497
1001-8417/

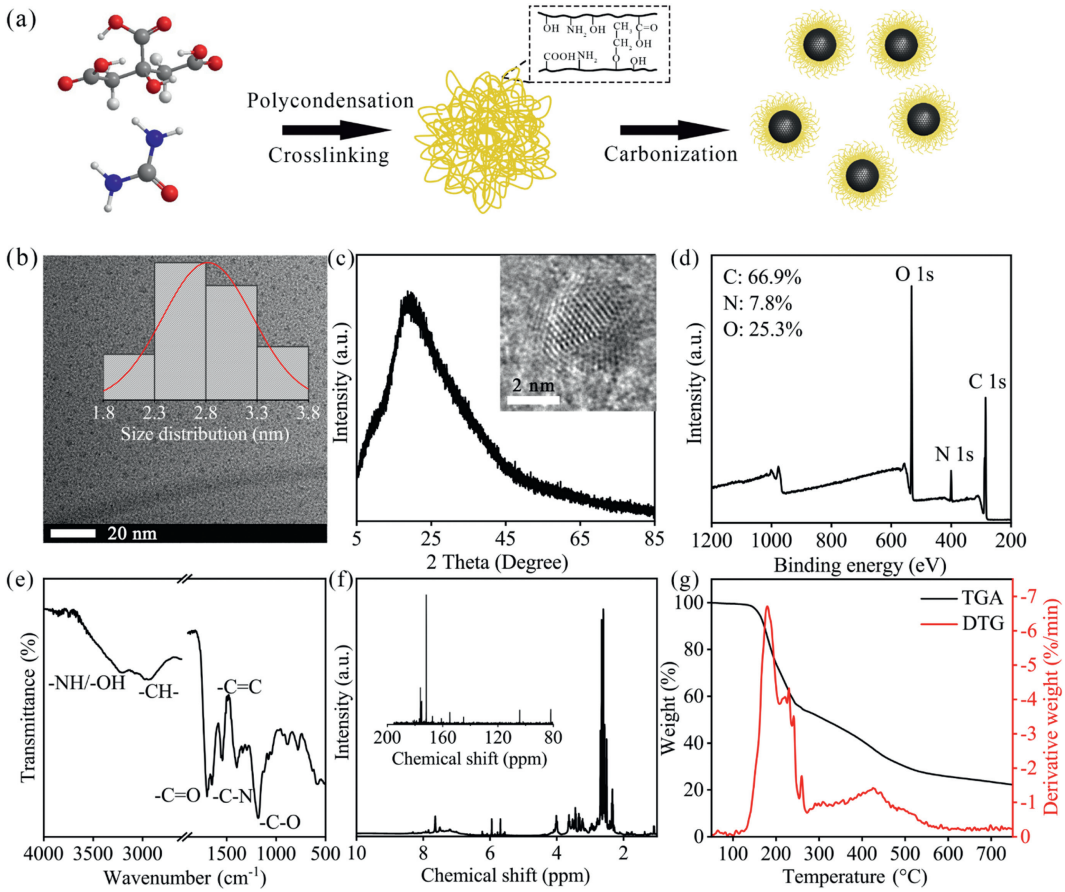

Fig. 1. Structural characterization of CDs. (a) Schematic illustrating the production process of the CDs. (b) TEM, (c) XRD patterns and HRTEM (inset), (d) XPS spectrum, (e) FTIR spectrum, (f) ^{1}H NMR spectrum and ^{13}C NMR (inset), and (g) TGA spectrum of CDs.

block blue light effectively and provide retina protection. This highlights that improving the quantum yield of yellow-light-emitting CDs substantially enhances their efficacy in blue light-blocking applications.

To overcome these challenges and broaden the application of CDs in blue light blocking, yellow light-emitting CDs were synthesized with a high quantum yield of 94% using urea and citric acid as precursors. These CDs exhibited minimal concentration dependence. Mixing CDs with polystyrene (PS) resulted in the production of CDs-based blue light-blocking films (CBF). By adjusting the proportion of CDs, varying degrees of blue light blocking capability were achieved in CBFs. Through their ability to absorb and convert light, these films effectively block the blue light wavelengths emitted by phones, WLEDs, and sunlight. These findings present a new alternative to conventional blue light-blocking films, offering material support for future research into next-generation displays and lighting devices focused on blue light protection.

As depicted in Fig. 1a, CDs were synthesized using citric acid and urea through a one-step solvothermal method, employing toluene as the reaction solvent. This method involves high temperature and pressure to carbonize the precursors effectively. Traditional hydrothermal methods typically yield blue-emitting CDs from the citric acid and urea system. Introducing toluene as an immiscible solvent facilitates the direct carbonization of citric acid and urea. The water produced during polycondensation quickly separates from toluene, promoting increased graphitization of the CDs and resulting in a red shift in the emission wavelength.

Following this, the CDs were characterized using transmission electron microscopy (TEM). TEM images in Fig. 1b illustrate the uniform shape of the CDs, with a 2.79 nm average particle size. High-resolution TEM (HRTEM) analysis confirmed the high crystallinity of the CDs [20], revealing lattice fringes with 0.21 nm spacing corresponding to the (001) plane of graphite carbon (inset of Fig. 1c). The X-ray diffraction (XRD) pattern of the CDs showed a distinct peak at approximately 21.1°, consistent with the XRD findings (Fig. 1c). Importantly, the XRD pattern of the CDs did not exhibit peaks from the precursors, indicating the high purity of the synthesized CDs. X-ray photoelectron spectroscopy (XPS) was utilized to analyze the elemental composition and chemical state of the CDs' surface. The XPS survey spectrum indicated the presence of carbon (C), nitrogen (N), and oxygen (O) at binding energies of 284.4, 398.5, and 531.6 eV, respectively [21]. The atomic percentages for these elements were 66.9%, 7.8%, and 25.3%, respectively (Fig. 1d). The HR C 1s spectrum of the CDs showed peaks at 284.4, 285.6, and 288.3 eV, corresponding to C–C/C=C, C–O/C–N, and C=O bonds, respectively [22]. The N 1s spectrum exhibited three component peaks at 399.0, 400.1, and 400.9 eV, representing pyridinic N, pyrrolic N, and graphitic N, respectively. In the HR O 1s spectrum, peaks were observed at 531.5 and 532.9 eV, indicative of C–O and C=O bonds, respectively (Fig. S1 in Supporting information). The functional groups on the CD surfaces were examined using Fourier transform infrared spectroscopy (FTIR). In the FTIR spectrum of the CDs (Fig. 1e), distinct peaks were observed corresponding to different functional groups: O–H/NH (3200–3400 cm^{-1}), C=O (1660 cm^{-1}), C=C (1480 cm^{-1}), C–N (1390 cm^{-1}), and C–O (1150 cm^{-1}) [23]. In the proton nuclear magnetic resonance (^{1}H NMR) spectrum of the CDs (recorded in DMSO–d_6, ppm). The signals of the uncarbonized precursors were detected in the range of

2–4 ppm, primarily originating from methyl and ethyl hydrogens. The multiple peak observed at 4.1 ppm can be attributed to the hydroxyl hydrogen in the $-CH_2-OH$ group. Aromatic hydrogen signals appear in the 6–8 ppm range, indicating the presence of both conjugated and non-conjugated carbon domains in the cross-linked carbon dots (Fig. 1f) [24]. The ^{13}C NMR spectrum further confirms the hybridized structure of the carbon dots, with signals around 140–150 ppm attributed to aromatic ring carbons, while the resonances between 160 ppm and 170 ppm indicate the presence of amide functional groups. Signals in the range of 170–180 ppm can be attributed to carboxyl functional groups (inset of Fig. 1f). This analysis suggests that the CDs exhibit a typical sp^2/sp^3 hybridization model, featuring numerous surface functional groups and side chains [25]. Thermogravimetric analysis (TGA) and derivative thermogravimetric analysis (DTG) were used to characterize the carbon cores and polymer features within the CDs (Fig. 1g). The CDs exhibited a typical one-step decomposition process, similar to that of conventional polymers, suggesting the incorporation of polymer chains. The DTG curve, which illustrates the rate of weight loss, displayed distinct peaks used to evaluate thermal degradation. Specifically, it revealed a two-stage degradation process of the CDs: Initial degradation occurred between 200 °C and 300 °C due to polymer chain breakdown, followed by a second stage around 450 °C involving the pyrolysis of internal cross-linked polymer chains and the polymer network. At 700 °C, the residual weight was 23%, indicating the weight percentage of the carbon cores within the CDs. These DTG findings support the presence of both polymer chains and carbon cores in the CDs [26].

Subsequently, the optical properties of the synthesized CDs were further explored in toluene. When dispersed in toluene, the purified CDs showed a single emission peak, demonstrating excitation-independent behavior (Fig. S2 in Supporting information) [27]. This emission peak was observed at 574 nm, with a quantum yield of 94.43% (Fig. S3 in Supporting information). When toluene is used as the solvent, citric acid, and urea are insoluble in toluene. At high temperatures, the precursors will accelerate carbonization to form a conjugated structure, thereby increasing its solubility in toluene. Compared with CDs prepared in polar solvents, this type of CDs has a higher degree of carbonization, so the emission wavelength will be red-shifted to the yellow light region. The UV absorption peak at 259 nm was due to the π-π^* electronic transition within the conjugated structure of the carbon core, while the absorption at 430 nm originated from the n-π^* electronic transition of C=O/C=N groups (Fig. 2a) [28]. The steady-state photoluminescence lifetime of the CDs was determined using single-photon counting. The decay curve of the CDs exhibited a fast component attributed to intrinsic state radiative recombination and a slow component corresponding to surface state recombination processes. The average lifetime measured was 8.48 ns (Fig. 2b). The extended fluorescence lifetime suggests

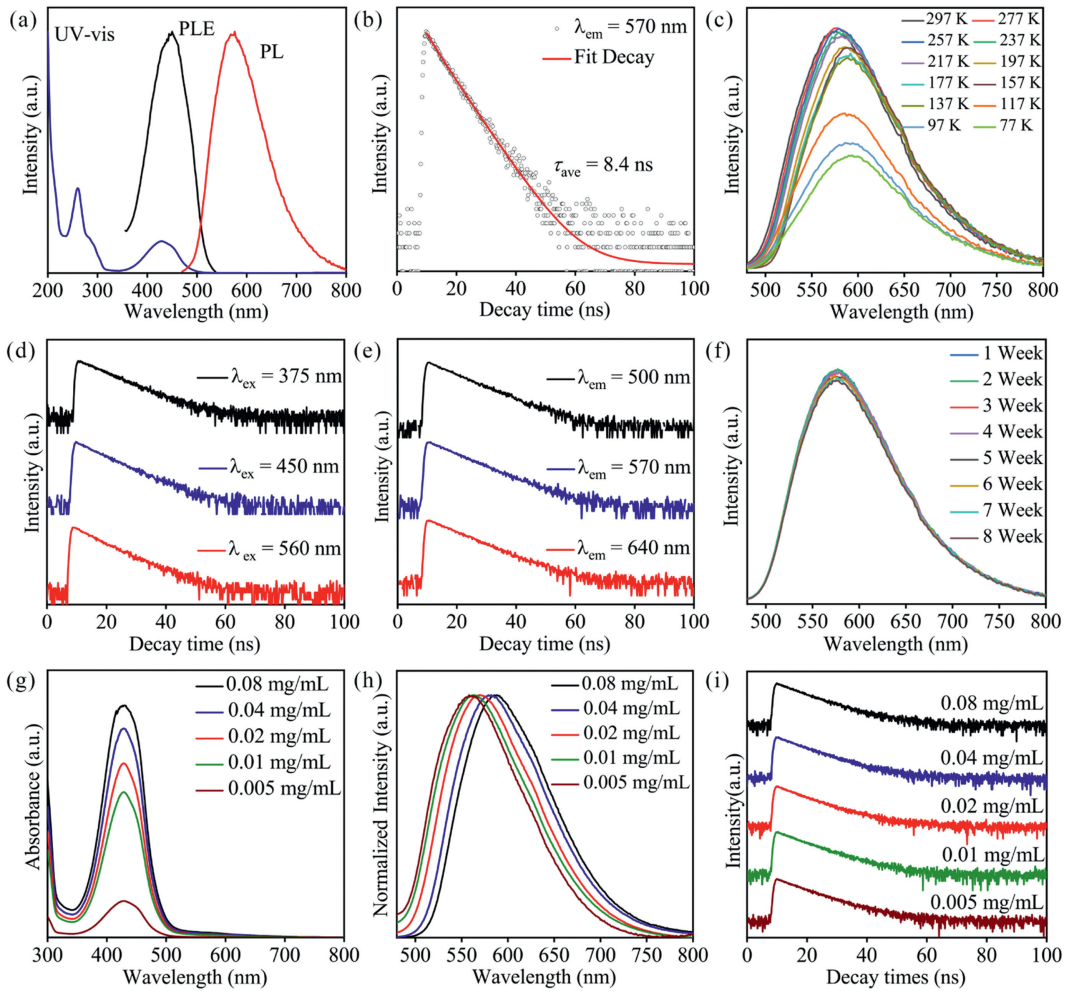

Fig. 2. Optical properties of CDs. (a) Absorption spectra, PL excitation, and emission spectra. (b) Fluorescence decay curve. (c) Temperature-dependent fluorescence spectra of CDs. (d) Fluorescence decay curve with different excitation (d) and emission (e) wavelength. (f) Storage stability of CDs solution. (g) UV absorption, (h) fluorescence emission, and (i) lifetime decay curves CDs with different concentrations.

a minimal non-radiative decay rate for the CDs, potentially contributing to their high quantum yield. Subsequently, temperature-dependent fluorescence spectra of the CDs solution were examined. As the temperature varied from freezing point to room temperature, a slight decrease in the fluorescence intensity of the CDs was observed, confirming their high quantum efficiency (Fig. 2c). During fluorescence decay measurements with varying excitation wavelengths, it was noted that shifting the excitation wavelength towards longer wavelengths resulted in a gradual increase in the fluorescence lifetime of the CDs. This phenomenon is attributed to the core-shell structure of CDs, where the carbon core states are typically deeper and more stable, with fewer non-radiative decay pathways (Fig. 2d and Table S1 in Supporting information). Longer-wavelength excitation primarily activates the deeper core states of CDs, thereby extending their fluorescence lifetime. Additionally, states excited by longer wavelengths tend to be more stable and exhibit fewer non-radiative decay pathways than those excited by shorter wavelengths. This reduced non-radiative decay enhances the probability of radiative decay, contributing to longer fluorescence lifetimes. Time-resolved emission spectra (TRES) indicated that CDs displayed consistent fluorescence decay processes across various emission wavelengths (Fig. 2e and Table S2 in Supporting information) [29]. This suggests that both absorption and subsequent emission processes follow uniform pathways, irrespective of the specific emission wavelength, ensuring consistent decay behavior. Importantly, the CDs showed remarkable long-term stability throughout a storage duration of 7 weeks at room temperature, as depicted in Fig. 2f. In addition, the concentration dependence of the as-prepared CDs was studied. The absorbance of the CDs exhibited a positive correlation with the concentration, suggesting that CDs possess adjustable light absorption properties within the blue spectral range (Fig. 2g). From Fig. 2h, it is evident that the emission wavelength exhibits a redshift as the CDs concentration increases. This aggregation-induced redshift is common in the field of CDs, primarily due to the stronger π-π interactions between the conjugated domains of adjacent CDs caused by aggregation. However, as the concentration increased, the fluorescence lifetime of the CDs also increased. This occurs because the distance between the CDs decreases at higher concentrations, facilitating energy transfer between particles. This energy transfer delays the emission process, effectively lengthening the observed fluorescence lifetime. Specifically, Förster Resonance Energy Transfer (FRET) can occur, where energy is transferred non-radiatively between closely spaced CDs, thus extending the fluorescence lifetime (Fig. 2i and Table S3 in Supporting information) [30].

By using the CDs' capacity to absorb short-wavelength light and emit long-wavelength light, the prepared CDs were mixed with PS and spin-coated to prepare CDs-based optical blocking films (CBFs). As the CD content increased from 1 wt% to 10 wt%, the normalized fluorescence spectrum of the CBFs remained nearly constant (Fig. 3a). The absorption spectra revealed a gradual increase in absorption intensity with higher CDs content in the CBFs, similar to

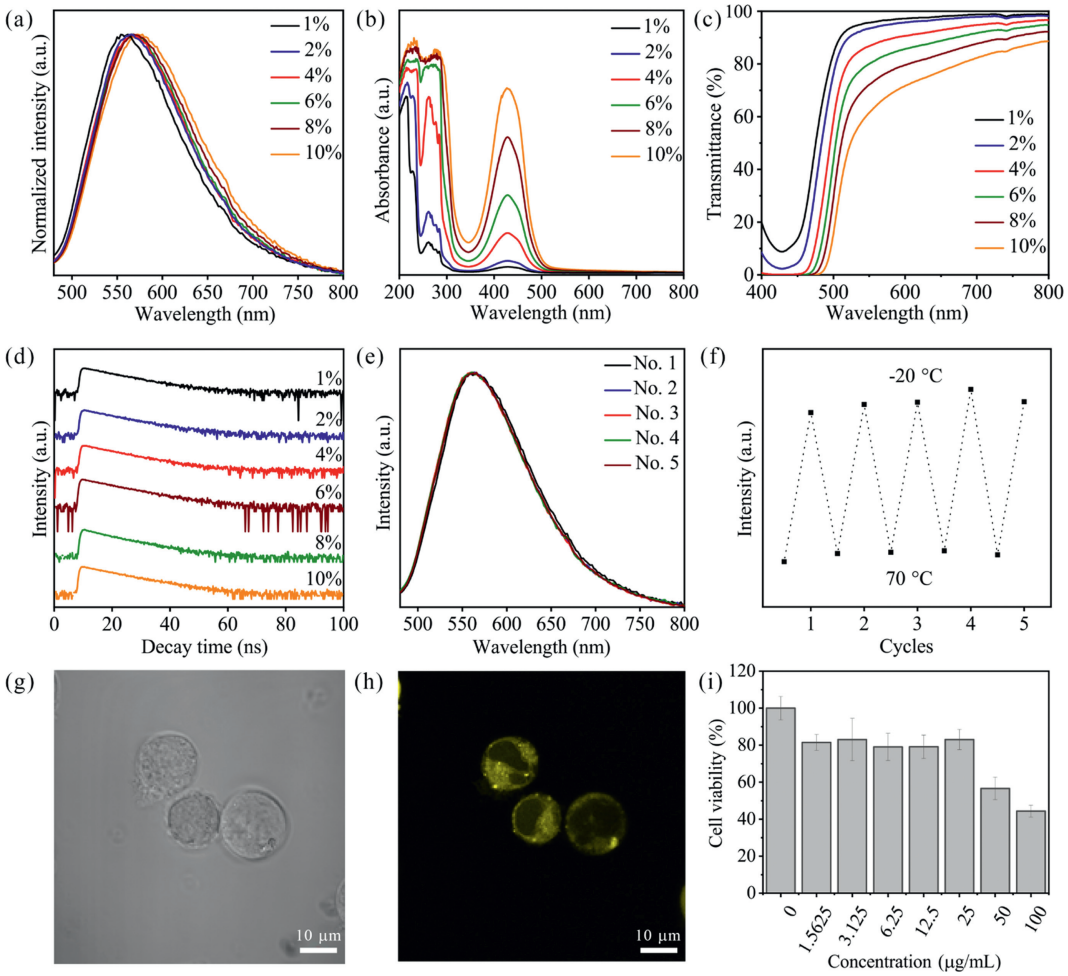

Fig. 3. Optical properties of CFBs. (a) PL emission, (b) UV–vis absorption, (c) transmittance, (d) fluorescence decay curve of CBFs. (e) PL emission spectra of CBFs at different locations over a large area. (f) Fluorescence intensity of CBFs with repeated cycling at −20 °C to 70 °C. Brightfield photomicrographs of the K562 cells incubated with CDs (g) and by excitation at 405 nm (h). (i) Cytotoxicity of CDs to K562 cells.

the behavior observed in CDs solution. Subsequently, the transmittance of the CBFs was evaluated (Fig. 3b). When the CDs were doped at 1%, the CBFs demonstrated effective absorption in the blue light region, thereby blocking blue light. As the CDs content increased, the transmittance at 450 nm decreased gradually, indicating enhanced absorption of light in the ultraviolet to blue spectral regions by the CBFs (Fig. 3c). When comparing the lifetimes of CBFs at different doping levels, an increase in CDs content led to longer lifetimes, which is consistent with the trend observed for CDs in solution (Fig. 3d and Table S4 in Supporting information). To enhance the commercial potential of CBFs, large-area films measuring 100 cm^2 were fabricated, making them suitable for blue-light blocking applications in mobile phones (Fig. 3e and Fig. S4 in Supporting information). The fluorescence intensity at five different positions on the large-area film was assessed using 365 nm excitation. These positions exhibited consistent fluorescence emission wavelengths and intensities, confirming the uniformity of the CBFs. Reversible fluorescence changes were observed over several heating and cooling cycles, demonstrating good heat and cold resistance, making CBFs suitable for everyday use (Fig. 3f). The decrease in fluorescence with increasing temperature was attributed to non-radiative transitions. Subsequently, to expand the application scenarios of CBFs, we analyzed the toxicity of the CDs to ensure their safety for daily use. Cellular immunofluorescence imaging and analysis experiments demonstrated the bioluminescence properties of CDs. Figs. 3g and h show brightfield and fluorescence images of human erythroleukemia cell line (K562) cells stained with CDs. Fluorescence images show uniform cytoplasmic staining in the cells and that CD can penetrate the nuclear membrane into the nucleus. CCK-8 performed the biological evaluation of CDs to detect the cytotoxicity of CDs against K562 cells, as shown in the above. The results showed that CDs acted on K562 cells at an IC_{50} of 108.9 μg/mL, indicating that K562 cells survived only 50% of CDs at 108.9 μg/mL. When the concentration of CDs is below 25 μg/mL, the K562 cell survival rate can reach 83%, which is less toxic to K562 cells (Fig. 3i).

To investigate the practical application of CBFs for blocking blue light, the ability of CBFs to block blue light emitted by an iPhone 15 screen was first measured (Fig. 4a). Comparing the blue light blocking capabilities of CBFs with varying CDs doping levels, it was observed that as the proportion of CDs increased, CBFs enhanced their ability to block blue light from the iPhone screen. This led to a gradual reduction in the proportion of transmitted blue light, accompanied by an increase in the green and red-light components. The CIE diagram (Fig. 4b) illustrates that with the increase in CDs, the spectrum of light emitted from the iPhone screen shifted from white light to warm white light, and eventually into the yellow light region. At the 1% doping level, the CDs were most effective in reducing blue light emission without causing color distortion. In another practical demonstration, a WLED was fabricated using CDs prepared in this study and a blue light-emitting chip (Fig. 4c). Applying CBFs over the WLEDs resulted in a gradual decrease in the peak intensity of the blue light chip as the CDs content increased. At a doping level of 10%, the film completely blocked the peak of the blue light chip, resulting in a shift in the CIE coordinates (Fig. 4d). The optical photographs of the WLEDs illustrated that as CDs doping increased, the WLEDs emitted yellow light (Fig. 4e). Finally, the ability of CBFs to block the blue light band in indoor natural light conditions was explored (Figs. 4f and g). CBFs demonstrated a similar blue light-blocking effect as observed with the phone screen and WLEDs. These findings confirm that CBFs, with their adjustable blue light blocking capabilities, can serve as

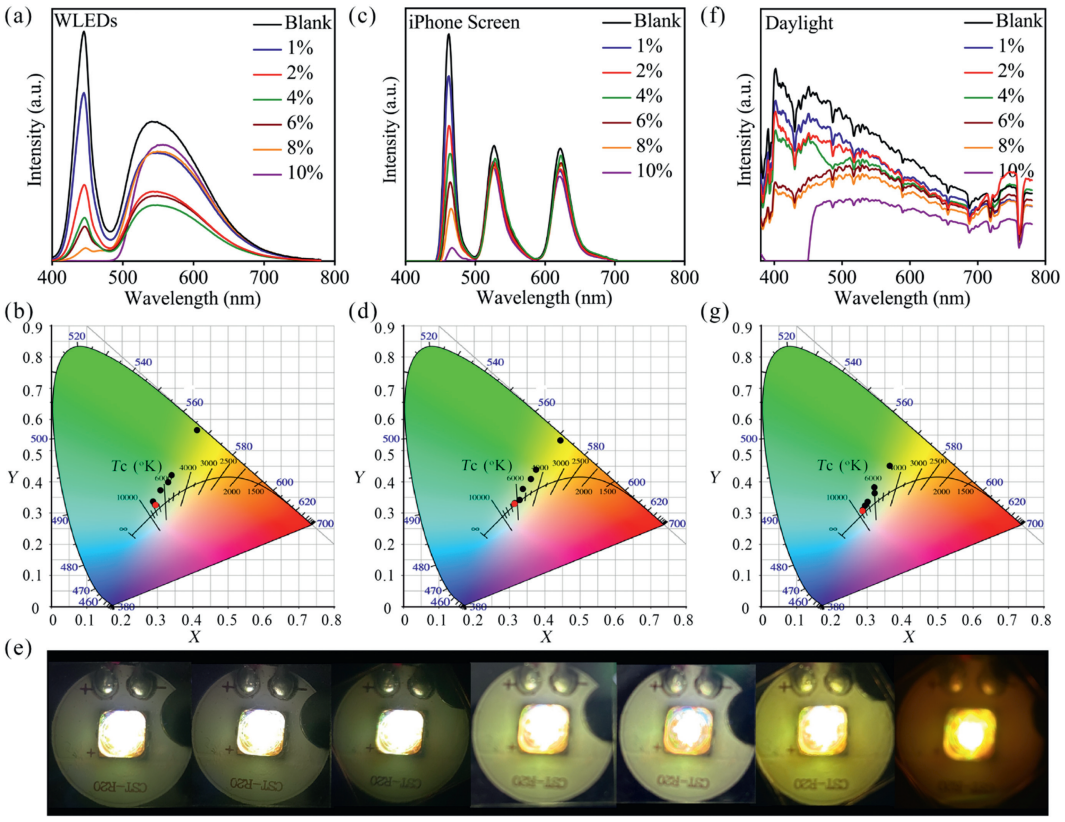

Fig. 4. Application of CBFs. Luminescence spectra of iPhone screens (a), WLEDs (c), and daylight (f) covered with different CDs-doped CBFs. CIE chromaticity coordinates of CBFs containing different proportions of CDs blocking blue light from iPhone screens (b), WLEDs (d), and daylight (g). (e) Photos of different CBFs coated onto WLEDs and energized.

effective films to protect human eyes from blue light damage. The film doped at 1% also exhibited high transmittance without causing color distortion, making it particularly suitable for commercial applications.

In summary, this study developed yellow-emitting CDs with high quantum yield and strong absorption capabilities in the blue light region. These CDs were subsequently integrated into polystyrene and fabricated into various CBFs with varying CDs contents using the spin-coating method. In contrast to traditional approaches, the spin-coated films exhibited superior uniformity, high transparency, and scalability. CBFs containing 1% CDs effectively filtered out blue light emitted by devices without altering the CIE coordinates, thereby preserving the light color. Furthermore, by changing the contents of CDs in the film, different levels of blue light-blocking CBFs can be made to meet different needs. The CBFs developed in this study have potential applications in blocking the harmful effects of blue light emitted by electronic devices in daily life.

Declaration of competing interest

The authors declare that they have no known competing financial interests or personal relationships that could have appeared to influence the work reported in this paper.

CRediT authorship contribution statement

Liwen Wang: Writing – original draft, Formal analysis, Data curation, Conceptualization. **Boyang Wang:** Formal analysis, Data curation, Conceptualization. **Siyu Lu:** Visualization, Validation, Investigation, Funding acquisition. **Shubo Lv:** Writing – review & editing, Supervision, Investigation. **Xiaoli Qu:** Validation, Supervision, Methodology, Investigation.

Acknowledgments

This work was supported by Medical Science and Technology Research Project of Henan Province (Joint Construction Project) (No. LHGJ20200433) and National Natural Science Foundation of China (No. 52122308).

Supplementary materials

Supplementary material associated with this article can be found, in the online version, at doi:10.1016/j.cclet.2024.110497.

References

[1] Y. Niwano, A. Iwasawa, K. Tsubota, et al., BMJ Open Ophthalmol. 4 (2019) e000217.
[2] I. Jaadane, G. Villalpando Rodriguez, P. Boulenguez, et al., Sci. Rep. 10 (2020) 6733.
[3] R. Akasov, E.V. Khaydukov, M. Yamada, et al., Adv. Drug Deliver. Rev. 184 (2022) 114198.
[4] M. Bonnans, L. Fouque, M. Pelletier, et al., J. Photoch. Photobio. B 212 (2020) 112026.
[5] B.K. Barman, Ø. Sele Handegård, A. Hashimoto, et al., ACS Sustain. Chem. Eng. 9 (2021) 9879–9890.
[6] S. Zhao, S. Zhu, H. Zhu, et al., Opt. Mater. 151 (2024) 115370.
[7] B. Su, J. Jin, Y. Peng, et al., Adv. Opt. Mater. 10 (2022) 2102619.
[8] S.J. Park, H.K. Yang, B.K. Moon, Nano Energy 60 (2019) 87–94.
[9] Q. Fu, Y. Qin, X. Zhang, et al., Ind. Crop. Prod. 217 (2024) 118897.
[10] J. Zhang, J. Yu, X. Wu, et al., Appl. Surf. Sci. 669 (2024) 160449.
[11] B. Wang, S. Lu, Matter 5 (2022) 110–149.
[12] B. Wang, G.I.N. Waterhouse, S. Lu, Trend. Chem. 5 (2023) 76–87.
[13] Y. Zhang, S. Lu, Chem 10 (2024) 134–171.
[14] H. Wang, L. Ai, H. Song, et al., Adv. Funct. Mater. 33 (2023) 2303756.
[15] L. Ai, W. Xiang, J. Xiao, et al., Adv. Mater. 36 (2024) 2401220.
[16] B. Wang, J. Yu, L. Sui, et al., Adv. Sci. 8 (2021) 2001453.
[17] B. Zhao, J. Ni, Y. Wang, et al., Dyes Pigments 223 (2024) 111947.
[18] Y. Han, X. Huang, J. Liu, et al., J. Colloid Interf. Sci. 617 (2022) 44–52.
[19] H. Guo, X. Zhang, Z. Chen, et al., Carbon 199 (2022) 431–438.
[20] B. Wang, J. Li, Z. Tang, et al., Sci. Bull. 64 (2019) 1285–1292.
[21] B. Wang, H. Song, Z. Tang, et al., Nano Res. 15 (2022) 942–949.
[22] M. Fang, B. Wang, X. Qu, et al., Chin. Chem. Lett. 35 (2024) 108423.
[23] B. Wang, H. Wang, B. Zhang, et al., Adv. Funct. Mater. 34 (2024) 2404437.
[24] B. Wang, H. Wang, Y. Hu, et al., Nano Lett. 23 (2023) 8794–8800.
[25] X. Yang, X. Li, B. Wang, et al., Chin. Chem. Lett. 33 (2022) 613–625.
[26] B. Wang, Z. Wei, L. Sui, et al., Light Sci. Appl. 11 (2022) 172.
[27] Z. Wei, B. Wang, M. Xie, et al., Chin. Chem. Lett. 33 (2022) 751–756.
[28] Y. Xu, B. Wang, M. Zhang, et al., Adv. Mater. 34 (2022) 2200905.
[29] B. Wang, H. Wang, Y. Hu, et al., Nano Lett. 24 (2024) 2904–2911.
[30] H. Song, X. Liu, B. Wang, et al., Sci. Bull. 64 (2019) 1788–1794.